This is an open access article published under an ACS AuthorChoice License, which permits copying and redistribution of the article or any adaptations for non-commercial purposes.

ACS Photonics
ACS Editors' Choice
Letter
pubs.acs.org/journal/apchd5

Amplitude- and Phase-Resolved Nanospectral Imaging of Phonon Polaritons in Hexagonal Boron Nitride

Zhiwen Shi,[†,¶] Hans A. Bechtel,[‡,¶] Samuel Berweger,[§,∥] Yinghui Sun,[†] Bo Zeng,[†] Chenhao Jin,[†] Henry Chang,[†] Michael C. Martin,[‡] Markus B. Raschke,[*,∥] and Feng Wang[*,†,⊥,#]

[†]Department of Physics, University of California at Berkeley, Berkeley, California 94720, United States

[‡]Advanced Light Source Division and [⊥]Materials Sciences Division, Lawrence Berkeley National Laboratory, Berkeley, California 94720, United States

[§]National Institute of Standards and Technology, Boulder, Colorado 80305, United States

[∥]Department of Physics, Department of Chemistry, and JILA, University of Colorado, Boulder, Colorado 80309, United States

[#]Kavli Energy NanoSciences Institute at the University of California, Berkeley, and the Lawrence Berkeley National Laboratory, Berkeley, California 94720, United States

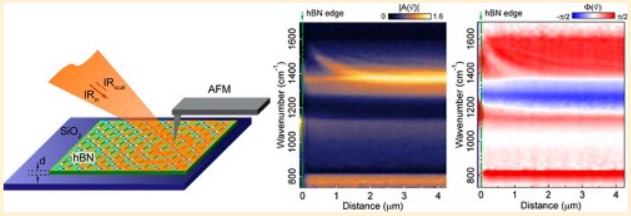

ABSTRACT: Phonon polaritons are quasiparticles resulting from strong coupling of photons with optical phonons. Excitation and control of these quasiparticles in 2D materials offer the opportunity to confine and transport light at the nanoscale. Here, we image the phonon polariton (PhP) spectral response in thin hexagonal boron nitride (hBN) crystals as a representative 2D material using amplitude- and phase-resolved scattering scanning near-field optical microscopy (*s*-SNOM) using broadband mid-IR synchrotron radiation. The large spectral bandwidth enables the simultaneous measurement of both out-of-plane (780 cm^{-1}) and in-plane (1370 cm^{-1}) hBN phonon modes. In contrast to the strong in-plane mode, the out-of-plane PhP mode response is weak. Measurements of the PhP wavelength reveal a proportional dependence on sample thickness for thin hBN flakes, which can be understood by a general model describing two-dimensional polariton excitation in ultrathin materials.

KEYWORDS: *phonon polariton, boron nitride, near-field spectroscopy, synchrotron infrared nanospectroscopy (SINS)*

Phonon polaritons[1] (PhPs) result from coupling of photons with optical phonons in polar crystals. Unlike *plasmon* polaritons,[2−4] which usually span a very broad energy range, PhPs provide a spectrally selective response related to the optical phonon modes in the infrared to terahertz spectral range. The PhPs can have strong spatial confinement and may enable potential applications for enhanced IR light−matter interaction,[5,6] high-density IR data storage,[7] coherent thermal emission,[8] development of metamaterials,[9,10] and frequency-tunable terahertz wave generation.[11]

Hexagonal boron nitride (hBN) is a convenient model system for studying PhPs in ultrathin materials because hBN flakes with different thicknesses are easy to prepare with high quality and no dangling bonds as a two-dimensional (2D) van der Waals material. It has two Reststrahlen bands in the mid-infrared region spanning the transverse (ω_{TO}) and longitudinal (ω_{LO}) phonon frequencies of the out-of-plane mode (ω_{TO} = 760, ω_{LO} = 825 cm^{-1}) and the in-plane mode (ω_{TO} = 1370, ω_{LO} = 1614 cm^{-1}). Both the lower frequency out-of-plane mode and the higher frequency in-plane mode have negative real parts of the dielectric function and thus have the potential to support PhPs.[12] Furthermore, hBN is a promising material for nanotechnology applications due to its 2D layered structure, excellent electrical insulation, and chemical and thermal stability. It has attracted great interest as a substrate for high-mobility graphene,[13−17] as an ideal dielectric layer and spacer for 2D heterostructures,[18,19] and for its intrinsic UV lasing response.[20]

Recently, the hBN PhP related behavior started to attract much interest.[21−24] Dai et al. studied PhPs in thin hBN flakes with laser-based scattering scanning near-field optical microscopy (*s*-SNOM) and observed a thickness-dependent PhP dispersion[21] in the upper spectral range around the in-plane (~1370 cm^{-1}) vibration phonon mode. However, they reported only spectral amplitude information on the coherent PhP response at the higher frequency in-plane phonon mode and relied on complex modeling to explain the thickness-dependent PhP dispersion. Here, we use broadband synchrotron infrared nanospectroscopy (SINS; see Methods)[25] for simultaneous amplitude and phase-resolved spatiospectral imaging of the PhPs in thin hBN flakes. We measure the PhP response for both the low-frequency out-of-plane (~780 cm^{-1}) and high-frequency in-plane (~1370 cm^{-1}) characteristic phonon modes of hBN. We describe the observed standing wave PhP behavior using a simple cavity model to

Received: January 12, 2015
Published: June 9, 2015

ACS Publications © 2015 American Chemical Society

DOI: 10.1021/acsphotonics.5b00007

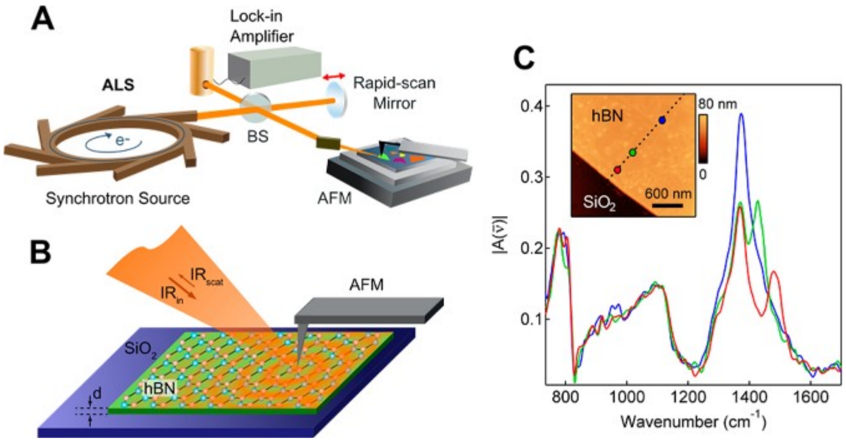

Figure 1. (A) Schematic of synchrotron infrared nanospectroscopy (SINS) using coherent broadband synchrotron infrared radiation provided by the Advanced Light Source (ALS) as the synchrotron source, a KBr beamsplitter (BS), and an atomic force microscope (AFM). (B) The synchrotron IR light illuminates the conductive AFM tip, which launches polariton waves that propagate radially outward from the tip along the hBN surface and are reflected off the edges, forming standing waves with the tip. (C) Representative amplitude $|A(\overline{\nu})|$ spectra taken from three different positions (marked with colored dots) of a 75 nm thick hBN flake, shown in the inset. A peak appears on the high-frequency side of the main in-plane phonon peak near 1370 cm^{-1} in the spectra taken near the hBN edge, due to the interference of the forward-moving and backward-moving polariton wave reflected by the hBN edge.

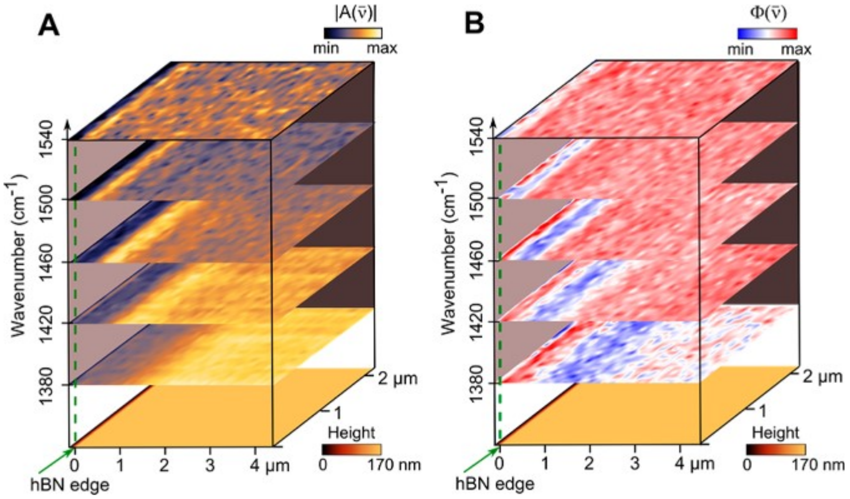

Figure 2. Sequence of real-space SINS images of near-field (A) amplitude $|A(\overline{\nu})|$ and (B) phase $\Phi(\overline{\nu})$ near an edge of a 160 nm thick hBN flake acquired simultaneously. The bottom image in both (A) and (B) is the topography of the sample, showing the sample edge on the left side of the image stack at $x = 0$ (indicated by the dotted green line). The color maps for the amplitude and phase images have been individually normalized to the maximum and minimum amplitude and phase value of each image for better visibility. Interference between the forward-propagating and back-reflected polariton waves modulates the near-field amplitude and phase as a function of the distance from the hBN edge. Different interference patterns are due to different polariton wavelengths.

simultaneously fit the amplitude and phase,[26] which allows us to extract the wavelength and reflection coefficients as they relate to the dispersion relation. We also develop a simple theory, general to 2D polaritons[27,28] in ultrathin layered materials, to describe the proportional dependence of the phonon polariton wavelength to sample thickness.[21]

Near-field Fourier transform infrared nanospectroscopy and imaging were performed with SINS at the Advanced Light Source.[25] In brief, broadband synchrotron IR light is focused onto the apex of a metal-coated atomic force microscope (AFM) tip with apex radius $r < 25$ nm (Figure 1A). The resulting large near-field momentum provided by the spatial field localization at the apex extends into the typical momentum range of hBN phonon polaritons and allows for their optical excitation. The excited polariton wave propagates radially outward from the near-apex launched region along the hBN surface (Figure 1B). When reaching the sample edge, the polariton waves are reflected. The back-reflected polariton waves interfere with the excitation field at the tip and modify the amplitude and the phase of the tip-scattered near-field, which is detected by interferometric heterodyne amplification.[25] This allows for the spatial and spectral imaging of the PhP waves. The strong dependence of the PhP wavelength on excitation frequency leads to a variation in the observed spectra, as shown in Figure 1C with three representative amplitude spectra taken at different distances from the edge of a 75 nm thick hBN flake.

To prepare samples, hBN[29] is directly exfoliated onto a SiO$_2$/Si (300 nm/500 μm) substrate with adhesive tape. The achieved hBN flake thickness varies from several atomic layers to hundreds of nanometers. After taking an AFM image of an hBN flake to determine its thickness, we either perform a single SINS line scan perpendicular to a straight edge or record full spatiospectral area scans in the edge region. Several specimens with thickness varying from 3 to 160 nm were measured and analyzed.

We measure both amplitude and phase of the BN phonon polariton near-field response. This provides for a consistency check given the inherent experimental uncertainty in *s*-SNOM measurements of phase and amplitude alone. In principle, amplitude and phase are Kramers−Kronig related. However, a unique phase assignment is difficult in general from an amplitude measurement alone (or vice versa) using the Kramers−Kronig relation, because the limited spectral range of the experiment does not allow for amplitude measurements over a broad enough frequency range for a unique spectral phase assignment. We therefore measure spectral amplitude and phase directly from the asymmetric near-field signal interferograms.[25]

Figure 2A and B show the real-space 2D mapping of the spectral near-field amplitude $|A(\overline{\nu})|$ and phase $\Phi(\overline{\nu})$ of a 160 nm thick hBN flake for selected excitation frequencies, respectively. The bottom images of Figure 2A and B are the topography of the sample; the straight edge is located on the left side ($x = 0$ μm). Interference between the forward-propagating and back-reflected polariton waves modulates the near-field amplitude and phase as a function of the distance from the hBN edge. Different interference patterns reflect different polariton wavelengths. All the interference patterns are parallel to the sample edge, showing uniform reflection of the PhP wave at the edge. Progressing from the top image to the bottom image, the maximum amplitude (Figure 2A) and minimum phase (Figure 2B) gradually move away from the hBN edge, due to the increase in polariton wavelength with decreasing incident IR frequency.

The large bandwidth of the synchrotron light enables us to simultaneously measure the near-field PhP IR response in a range that covers both the in-plane and out-of-plane phonon modes. Figure 3A and B show broadband spatiospectral maps of near-field amplitude and phase, respectively, for a line scan perpendicular to the edge of the sample. Increased scattering amplitudes (Figure 3A) around 1370 and 780 cm^{-1} correspond to the hBN in-plane and out-of-plane phonon modes, respectively, and the spectral feature around 1130 cm^{-1} is due to the SiO$_2$ phonon of the substrate.[25,27] Spatially dependent features arising from propagating polaritons show up between the transverse (ω_{TO}) and longitudinal (ω_{LO}) optical phonon frequencies in both the in-plane and out-of-plane phonon modes (Figure 3A and B). This phenomenon is revealed more clearly in Figure 3C and D with five spectra at the positions marked with dashed lines in Figure 3A and B, respectively. For the in-plane phonon mode, the main peak at ∼1370 cm^{-1} remains largely unchanged in Figure 3C, while the interference peak on the right shoulder of the main phonon peak moves progressively to lower frequency as the tip scans farther from the sample edge. Likewise, the main phonon peak of the out-of-plane phonon mode at ∼770 cm^{-1} remains largely unchanged, but in this case, the interference peak moves progressively to higher frequency as the tip scans farther from the sample edge. A similar PhP behavior is observed for both modes in the near-field phase spectra presented in Figure 3D.

To highlight these changes in PhP wavelength with excitation frequency, we show expanded views of the hBN in-plane and out-of-plane spectral regions in Figures 4 and 5, respectively, along with distance profiles at representative excitation frequencies. These distance profiles clearly show the interference between the forward and back-reflected PhP waves in both the amplitude and phase responses. For the in-plane mode, the PhP wavelength is longest at low frequencies and becomes progressively shorter as the excitation frequency approaches the $\omega_{\mathrm{LO}} = 1614$ cm^{-1} limit, whereas for the out-of-plane limit, the PhP wavelength is shortest at low frequencies and becomes progressively longer as the excitation frequency approaches the $\omega_{\mathrm{LO}} = 825$ cm^{-1} limit. This behavior is consistent with the fact that hBN is a natural hyperbolic material, whose in-plane and out-of-plane real part of dielectric functions are of opposite sign in a certain energy range related to its phonon modes.[30] In hBN, the lower frequency out-of-plane mode is a type I hyperbolic mode with $\mathrm{Re}(\varepsilon_{\perp}) < 0$ and $\mathrm{Re}(\varepsilon_{\parallel}) > 0$, whereas the higher frequency in-plane mode is a type II hyperbolic mode with $\mathrm{Re}(\varepsilon_{\perp}) > 0$ and $\mathrm{Re}(\varepsilon_{\parallel}) < 0$. hBN thus has both types of hyperbolic response in the same sample. The two types of hyperbolic modes have different PhP wavelength dispersion relations with respect to the excitation frequency, with type I modes illustrating an ascending behavior, in which the polariton wavelength increases with excitation frequency, and type II

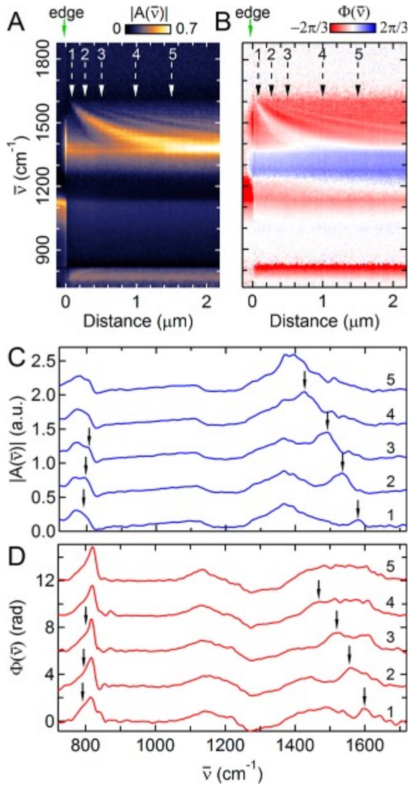

Figure 3. Spatiospectral SINS line scan of hBN phonon polaritons with spectral cuts. Simultaneously acquired (A) near-field amplitude $|A(\overline{\nu})|$ and (B) phase $\Phi(\overline{\nu})$ linescan obtained perpendicular to the edge of a 147 nm thick hBN flake. The green arrow at $x = 0$ marks the edge of the hBN crystal. Signals around 1370 and 780 cm^{-1} correspond to the in-plane and out-of-plane phonon mode in hBN, respectively, and the signal around 1130 cm^{-1} is related to the SiO$_2$ phonon mode of the substrate. Strong PhP features only appear around the in-plane phonon mode (1370 cm^{-1}). Near-field (C) amplitude and (D) phase spectra at five representative positions, marked in (A) and (B).

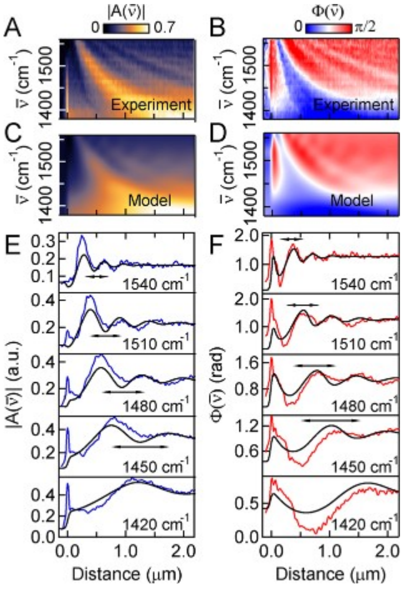

Figure 4. Cavity model analysis of experimental spatial and spectral profiles. Experimental (A) SINS amplitude $|A(\bar{\nu})|$ and (B) phase $\Phi(\bar{\nu})$ spatiospectral linescan in the region of the hBN in-plane phonon mode of the 147 nm thick hBN flake. Note the different color scales from Figure 3 with absolute phase values. Simulated SINS (C) amplitude and (D) phase spatiospectral linescan of the same hBN flake in (A) and (B) using the cavity model discussed in the text. (E) Experimental (blue) and simulated SINS amplitude (black) distance profiles extracted from (A) and (C), respectively. (F) Experimental (red) and simulated SINS phase (black) distance profiles extracted from (B) and (D), respectively.

modes exhibiting a descending behavior, with the wavelength decreasing with excitation frequency.

The distance profiles of the amplitude and phase measurements in Figure 4C and D show consistent patterns in which the maximum phase response occurs at the edge of the flake, whereas the maximum amplitude response is displaced from the edge. In the following, we describe the observed near-field amplitude and phase self-consistently using a simple cavity model formed between the PhP launching and scattering tip and propagating PhP reflecting the hBN crystal edge. As discussed in detail elsewhere,[26] we model the complex-valued substrate response $\tilde{\Psi}$ from the dielectric sample response $\tilde{\psi}_{\mathrm{hBN}}$, the resonant local PhP response $\tilde{\psi}_{\mathrm{PhP},0}$, and the reflected PhP response $\tilde{\psi}_{\mathrm{PhP},1}$ as $\tilde{\Psi} = \tilde{\psi}_{\mathrm{hBN}} + \tilde{\psi}_{\mathrm{PhP},0} + \tilde{\psi}_{\mathrm{PhP},1}$. To account for the spatial averaging by the tip, we convolve the sample response with a weighting function Θ to yield the modeled signal $\tilde{A}(r) = \tilde{\Psi}(r') \times \Theta(r - r')$. To approximate the tip geometry, we use a Gaussian function for Θ with a width of 30 nm. We then fit the wavelength-dependent amplitude and phase simultaneously using this cavity model. Figure 4A and B show the experimental PhP response from 1380 to 1560 cm^{-1}, and Figure 4C and D show the corresponding results of the fit. Further shown in Figure 4E and F are line cuts at select frequencies with the experimentally measured tip–edge distance dependencies of $|A(\bar{\nu})|$ (E) and phase $\Phi(\bar{\nu})$ (F), in blue and red, respectively, and the fit results (black). From the fitting, we can estimate the polariton wavelength, reflection coefficients, and damping. We typically find a reflection coefficient of $R = -1$ (corresponding to a reflection phase of π) at the hBN edge. (The reflection coefficient and phase have large uncertainty due to the low polariton quality factor and the uncertainty in defining the exact position of the hBN edge.) However, for the case of lower frequency PhP modes (1480, 1450, and 1420 cm^{-1}) the increase in amplitude near the edge as seen in Figure 4E suggests the possibility of a change in reflection coefficient. The bright amplitude response at $x = 0$ may result from a change in the interaction geometry, whereby the tip interacts with the vertical edge of the flake, but could also be caused by the generation of PhPs at the edge itself. However, in contrast to the much stronger polarizability of the metallic tip, this edge contribution is expected to be weak and therefore neglected in our analysis. Further theoretical investigation will be required for a complete description of the PhP response and to fully understand the PhP reflection and its phase behavior at the hBN edges across the whole spectral range.

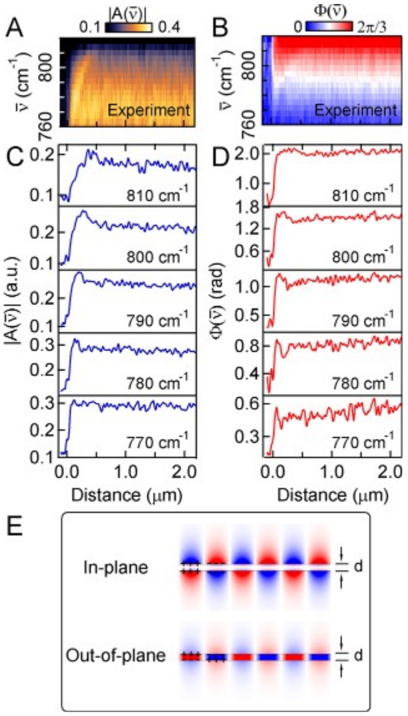

Figure 5. Experimental (A) SINS amplitude $|A(\bar{\nu})|$ and (B) phase $\Phi(\bar{\nu})$ spatiospectral linescan in the region of the hBN out-of-plane phonon mode of the 147 nm thick hBN flake. Experimental amplitude (C) and phase (D) distance profiles extracted from (A) and (B), respectively. (E) Color map of the electrical field along the *c*-axis for the fundamental in-plane (top) and out-of-plane (bottom) phonon polariton modes.

As noted above, hBN is a natural hyperbolic material, and in bulk hBN, many waveguide modes of phonon polaritons can exist. Their description requires the full knowledge of both the in-plane and out-of-plane dielectric constants.[21,22] However, in the 2D limit, where the hBN flake thickness can be a few tens of nanometers or even a few atomic layers, the only observable mode in our near-field microscopy study is the fundamental mode. All the other modes will have wavelengths shorter than or comparable to the film thickness because they require at least one full oscillation over the film thickness. The higher order polaritons, due to their very short wavelengths, are strongly confined in the bulk and do not couple efficiently to an external scattering center in the form of the tip in this case, and thus are not observed in our near-field experiment.

DOI: 10.1021/acsphotonics.5b00007
ACS Photonics 2015, 2, 790–796

Similarly, the observed out-of-plane mode PhP response is weak (Figures 3, 5) as compared to the higher frequency in-plane mode PhP response (Figures 3, 4). Figure 5E is a schematic of the electrical field (along the *c*-axis or *z*-direction) distribution. The fundamental mode of in-plane PhP features the same sign of charge accumulated at the top and bottom surfaces of a thin BN flake, while the fundamental mode of the out-of-plane PhP features charge accumulation with opposite signs at the two surfaces. For the in-plane PhP mode, the electrical field is mainly outside the 2D material (Figure 5E, top panel); for the out-of-plane PhP mode, the electrical field is mainly concentrated inside the hBN flake. For ultrathin hBN flakes at the 2D limit with $\lambda \gg d$, the polariton with opposite sign of charge at the top and bottom surfaces does not couple efficiently to the tip because the electrical field is strongly confined inside the 2D material. Therefore, the observed PhP feature for the out-of-plane mode is much weaker, and this effect becomes even stronger when the BN layer becomes thinner. Indeed, within our signal-to-noise ratio, we do not observe PhP features in the out-of-plane mode for thicknesses $d < 70$ nm.

Besides the 160 nm thick and the 147 nm thick samples, we systematically measured a set of samples with thicknesses from 3 to 160 nm. Spatiospectral maps of near-field amplitude and phase at the in-plane phonon mode for three more samples with thicknesses of 7, 22, and 40 nm are displayed in Figure 6A and B. The gradual change of the in-plane PhP feature with sample thickness is clearly seen and is caused by the variation of polariton wavelength with hBN crystal thickness. Figure 6C shows the dependence of the polariton wavelengths λ_p on sample thickness d for three selected frequencies at $\bar{\nu} = 1410$, 1440, and 1470 cm^{-1}, exhibiting linear scaling behavior for all frequencies.

To understand the experimentally observed scaling behavior for the in-plane PhP mode, we present a general model describing 2D polaritons in ultrathin materials where the thickness d is much smaller than the polariton wavelength λ_p. 2D polaritons are characterized by in-plane charge density oscillations, which generate an appreciable electrical field distribution near the surface that can couple efficiently to a tip via its near-field. The elementary charge oscillations can arise from free electrons, ions, and excitons, known respectively as plasmon, phonon, and exciton polaritons. In contrast, out-of-plane charge density oscillations generate a large electric field inside the 2D material, but the field outside the material is negligible (at the level of d/λ_p). Such out-of-plane modes, like the 780 cm^{-1} phonon in hBN, do not couple efficiently to a near-field probe and, thus, are less easily observed in our experiment.

For 2D polaritons associated with in-plane charge oscillations, the physics is uniquely determined by a single parameter□ the in-plane 2D susceptibility $\chi^{2D} = \chi_{\parallel}^{bulk} d = (\varepsilon_{\parallel}^{bulk} - 1)d$□ because the electrical field for the fundamental PhP mode in ultrathin hBN flakes is mainly in plane. Here $\chi_{\parallel}^{bulk}$ and $\varepsilon_{\parallel}^{bulk}$ are the in-plane bulk susceptibility and dielectric constant, respectively. The dispersion relation of 2D polaritons (in the long-wavelength limit) is then simply determined by a zero dynamical screening function $1 + \varepsilon_0(q^2/e)\, \chi^{2D}(\omega)\, \nu_c^{2D}(q) = 0$,[31] where $\nu_c^{2D}(q) = e/(2\varepsilon_0\varepsilon_{eff}\, q)$ is the 2D Coulomb interaction, $q = 2\pi/\lambda_p$ is the polariton wavevector, and ε_{eff} is the effective dielectric constant due to the environmental screening. Consequently, we obtain a simple yet general solution for 2D polariton dispersion in ultrathin films of $\lambda_p = -(\pi d/\varepsilon_{eff})[\varepsilon_{\parallel}^{bulk}(\omega) - 1]$. This simple model correctly predicts the linear scaling behavior between the phonon polariton wavelength λ_p and the thickness d for a given frequency in thin hBN crystals (Figure 6C; here the value of the hBN dielectric function $\varepsilon_{\parallel}^{bulk}(\omega)$ is from ref 11). It also shows that a 2D phonon polariton is independent of the perpendicular dielectric constant $\varepsilon_{\perp}^{bulk}(\omega)$ in thin crystals. Using an effective environmental dielectric constant $\varepsilon_{eff} = (\varepsilon_{air} + \varepsilon_{SiO_2})/2$, our theory qualitatively reproduces the experimentally observed dispersion relation (Figure 6D). The deviation between theory and experimental data mainly originates from the inaccuracy of ε_{eff} from neglecting the silicon substrate (300 nm away from the hBN layer) contribution, which is polariton wavelength dependent. The theoretical model is a good approximation only when the sample thickness is much smaller than the polariton wavelength. However, in addition to its application to PhPs in hBN, we expect this simple model to provide a good general description of any 2D polariton system, including plasmon polaritons in graphene, as well as phonon or exciton polaritons in other ultrathin crystals.

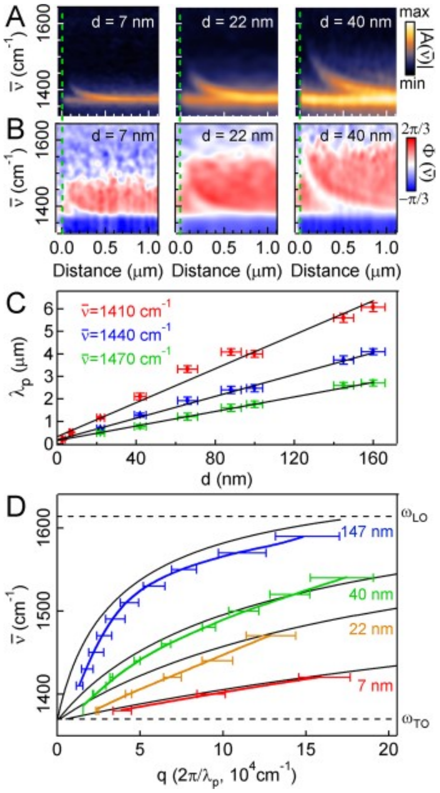

Figure 6. PhP dispersion and evolution of the in-plane phonon polariton wavelength with sample thickness. Spatiospectral maps of (A) SINS amplitude $|A(\bar{\nu})|$ and (B) phase $\Phi(\bar{\nu})$ for samples with thicknesses of 7, 22, and 40 nm. (C) Evolution of the in-plane phonon polariton wavelength, λ_p, with sample thickness, d, at three representative excitation frequencies: 1410, 1440, and 1470 cm^{-1}. For thin hBN flakes, λ_p is proportional to sample thickness. (D) Experimental (colored curves) and theoretical (black curves) dispersion relations of in-plane PhPs on hBN flakes with different thicknesses. The horizontal dashed lines are the longitudinal ($\omega_{LO} = 1614$ cm^{-1}) and transverse ($\omega_{TO} = 1370$ cm^{-1}) optical phonon frequencies of hBN.

In summary, we have investigated phonon polaritons in hBN crystals of different thicknesses by using broadband synchrotron infrared near-field spectroscopy and imaging. We find that in the measured hBN basal plane a strong PhP response is observed only around the in-plane phonon mode, and the measured polariton wavelength is proportional to sample thickness. In contrast to the strong in-plane mode, the out-of-plane mode PhP response is weak. The observed scaling behavior for the in-plane phonon polariton mode can be well understood with a simple theory that is universal for polaritons in thin 2D materials. Our results open up new avenues in engineering infrared light at the nanometer scale for novel photonic nanodevices and understanding intriguing polariton behaviors in low-dimensional nanomaterials.

METHODS

Approximately 500 μW of broadband synchrotron IR light from Beamline 5.4 at the Advanced Light Source (ALS) of Lawrence Berkeley National Laboratory is coupled to an asymmetric Michelson interferometer, consisting of a 50:50 KBr/Ge beamsplitter (Thermo-Scientific), a modified commercial AFM (Innova, Veeco/Bruker), and a modified commercial FTIR spectrometer (Nicolet 6700, Thermo-Scientific). The beamsplitter directs half of the light to the scanning mirror in the FTIR spectrometer and directs the other half to a parabolic mirror (N.A. $\approx$ 0.4) that focuses the beam onto a platinum silicide (PTSi-NCH, Nanosensors) AFM tip. The backscattered light from the AFM tip, collected by the same parabolic mirror, and the light reflected from the moving mirror are recombined on the beamsplitter and focused onto an MCT detector (KLD-0.1-J1, Kolmar). The AFM is operated in noncontact mode, and the tip-scattered signal is demodulated at twice the tip-oscillation frequency (typically 250−300 kHz) with a lock-in amplifier (HF2Li-MF, Zurich Instruments).[32,33] Spectra are acquired with interferometric heterodyne detection by moving the mirror in the modified FTIR spectrometer.[25] The broad spectral range of the synchrotron source enables the acquisition of spectra across the entire mid-IR range (700−5000 cm^{-1}) within a single scan. The Fourier transform of the resulting interferograms results in the complex-valued near-field spectrum. The real and imaginary spectra, typically represented as spectral amplitude and phase, relate to the complex dielectric function of the material.[33,34]

AUTHOR INFORMATION

Corresponding Authors

*E-mail: fengwang76@berkeley.edu.
*E-mail: markus.raschke@colorado.edu.

Author Contributions

Y.S. and Z.S. exfoliated the thin hBN samples. Z.S., H.A.B., Y.S., B.Z., and C.J. performed the near-field optical measurements. M.B.R., H.A.B., and M.C.M. developed SINS at the ALS. S.B. and M.B.R. developed the PhP near-field tip-boundary cavity model. H.A.B., Z.S., S.B., B.Z., H.C., and M.B.R. analyzed the data and made the figures. Z.S., H.A.B., F.W., S.B., and M.B.R. wrote the paper. F.W. developed the 2D polariton theory, conceived the experiment, and led the study. F.W., M.B.R., and M.C.M. supervised the project. All authors discussed the results.

Author Contributions

¶Z. Shi and H. A. Bechtel contributed equally to this work.

Notes

The authors declare no competing financial interest.

ACKNOWLEDGMENTS

Sample preparation and optical measurements in this work were mainly supported by the Office of Naval Research (award N00014-13-1-0464). F.W. acknowledges support from a David and Lucile Packard fellowship. The ALS is supported by the Director, Office of Science, Office of Basic Energy Sciences, and the BSISB is supported by the Office of Biological and Environmental Research, all through the U.S. Department of Energy (DOE) under Contract No. DE-AC02-05CH11231. M.R. acknowledges supported by the U.S. DOE, Office of Basic Energy Sciences, Division of Materials Sciences and Engineering, under Award No. DE-FG02-12ER46893. Mention of commercial products is for informational purposes only; it does not imply NIST's recommendation or endorsement.

REFERENCES

(1) Claus, R.; Merten, L.; Brandmüller, J. *Light Scattering by Phonon-Polaritons*; Springer-Verlag, 1975.

(2) Barnes, W. L.; Dereux, A.; Ebbesen, T. W. Surface plasmon subwavelength optics. *Nature* **2003**, *424*, 824−830.

(3) Gramotnev, D. K.; Bozhevolnyi, S. I. Plasmonics beyond the diffraction limit. *Nat. Photonics* **2010**, *4*, 83−91.

(4) El-Sayed, I. H.; Huang, X. H.; El-Sayed, M. A. Surface plasmon resonance scattering and absorption of anti-EGFR antibody conjugated gold nanoparticles in cancer diagnostics: applications in oral cancer. *Nano Lett.* **2005**, *5*, 829−834.

(5) Hillenbrand, R.; Taubner, T.; Keilmann, F. Phonon-enhanced light-matter interaction at the nanometre scale. *Nature* **2002**, *418*, 159−162.

(6) Anderson, M. S. Enhanced infrared absorption with dielectric nanoparticles. *Appl. Phys. Lett.* **2003**, *83*, 2964−2966.

(7) Ocelic, N.; Hillenbrand, R. Subwavelength-scale tailoring of surface phonon polaritons by focused ion-beam implantation. *Nat. Mater.* **2004**, *3*, 606−609.

(8) Greffet, J. J.; Carminati, R.; Joulain, K.; Mulet, J. P.; Mainguy, S.; Chen, Y. Coherent emission of light by thermal sources. *Nature* **2002**, *416*, 61−64.

(9) Schuller, J. A.; Zia, R.; Taubner, T.; Brongersma, M. L. Dielectric metamaterials based on electric and magnetic resonances of silicon carbide particles. *Phys. Rev. Lett.* **2007**, *99*, 107401.

(10) Shvets, G. Photonic approach to making a material with a negative index of refraction. *Phys. Rev. B* **2003**, *67*, 035109.

(11) Tanabe, T.; Suto, K.; Nishizawa, J.; Saito, K.; Kimura, T. Frequency-tunable terahertz wave generation via excitation of phonon-polaritons in GaP. *J. Phys. D: Appl. Phys.* **2003**, *36*, 953−957.

(12) Geick, R.; Perry, C. H.; Rupprech, G. Normal modes in hexagonal boron nitride. *Phys. Rev.* **1966**, *146*, 543.

(13) Dean, C. R.; Young, A. F.; Meric, I.; Lee, C.; Wang, L.; Sorgenfrei, S.; Watenabe, K.; Taniguchi, T.; Kim, P.; Shepard, K. L.; Hone, J. Boron nitride substrates for high-quality graphene electronics. *Nat. Nanotechnol.* **2010**, *5*, 722−726.

(14) Yang, W.; Chen, G.; Shi, Z.; Liu, C. C.; Zhang, L.; Xie, G.; Cheng, M.; Wang, D.; Yang, R.; Shi, D.; Watanabe, K.; Taniguchi, T.; Zhang, Y.; Zhang, G. Epitaxial growth of single-domain graphene on hexagonal boron nitride. *Nat. Mater.* **2013**, *12*, 792−797.

(15) Ponomarenko, L. A.; Gorbachev, R. V.; Yu, G. L.; Elias, D. C.; Jalil, R.; Patel, A. A.; Mishchenko, A.; Mayorov, A. S.; Woods, C. R.; Wallbank, J. R.; Mucha-Kruczynski, M.; Piot, B. A.; Potemski, M.; Grigorieva, I. V.; Novoselov, K. S.; Guinea, F.; Fal'ko, V. I.; Geim, A. K. Cloning of Dirac fermions in graphene superlattices. *Nature* **2013**, *497*, 594−597.

(16) Dean, C. R.; Wang, L.; Maher, P.; Forsythe, C.; Ghahari, F.; Gao, Y.; Katoch, J.; Ishigami, M.; Moon, P.; Koshino, M.; Taniguchi, T.; Watanabe, K.; Shepard, K. L.; Hone, J.; Kim, P. Hofstadter's butterfly and the fractal quantum Hall effect in moire superlattices. *Nature* **2013**, *497* (7451), 598−602.

(17) Hunt, B.; Sanchez-Yamagishi, J. D.; Young, A. F.; Yankowitz, M.; LeRoy, B. J.; Watanabe, K.; Taniguchi, T.; Moon, P.; Koshino, M.; Jarillo-Herrero, P.; Ashoori, R. C. Massive Dirac fermions and Hofstadter butterfly in a van der Waals heterostructure. *Science* **2013**, *340* (6139), 1427−1430.

(18) Levendorf, M. P.; Kim, C. J.; Brown, L.; Huang, P. Y.; Havener, R. W.; Muller, D. A.; Park, J. Graphene and boron nitride lateral heterostructures for atomically thin circuitry. *Nature* **2012**, *488* (7413), 627−632.

(19) Liu, L.; Park, J.; Siegel, D. A.; McCarty, K. F.; Clark, K. W.; Deng, W.; Basile, L.; Idrobo, J. C.; Li, A. P.; Gu, G. Heteroepitaxial growth of two-dimensional hexagonal boron nitride templated by graphene edges. *Science* **2014**, *343* (6167), 163−167.

(20) Kubota, Y.; Watanabe, K.; Tsuda, O.; Taniguchi, T. Deep ultraviolet light-emitting hexagonal boron nitride synthesized at atmospheric pressure. *Science* **2007**, *317*, 932−934.

(21) Dai, S.; Fei, Z.; Ma, Q.; Rodin, A. S.; Wagner, M.; McLeod, A. S.; Liu, M. K.; Gannett, W.; Regan, W.; Watanabe, K.; Taniguchi, T.; Thiemens, M.; Dominguez, G.; Castro Neto, A. H.; Zettl, A.; Keilmann, F.; Jarillo-Herrero, P.; Fogler, M. M.; Basov, D. N. Tunable phonon polaritons in atomically thin van der Waals crystals of boron nitride. *Science* **2014**, *343* (6175), 1125−1129.

(22) Caldwell, J. D.; Kretinin, A. V.; Chen, Y. G.; Giannini, V.; Fogler, M. M.; Francescato, Y.; Ellis, C. T.; Tischler, J. G.; Woods, C. R.; Giles, A. J.; Hong, M.; Watanabe, K.; Taniguchi, T.; Maier, S. A.; Novoselov, K. S. Sub-diffractional volume-confined polaritons in the natural hyperbolic material hexagonal boron nitride. *Nat. Commun.* **2014**, *5*, 6221.

(23) Xu, X. J. G.; Ghamsari, B. G.; Jiang, J. H.; Gilburd, L.; Andreev, G. O.; Zhi, C. Y.; Bando, Y.; Golberg, D.; Berini, P.; Walker, G. C. One-dimensional surface phonon polaritons in boron nitride nanotubes. *Nat. Commun.* **2014**, *5*, 5782.

(24) Brar, V. W.; Jang, M. S.; Sherrott, M.; Kim, S.; Lopez, J. J.; Kim, L. B.; Choi, M.; Atwater, H. Hybrid surface-phonon-plasmon polariton modes in graphene/monolayer h-BN heterostructures. *Nano Lett.* **2014**, *14* (7), 3876−3880.

(25) Bechtel, H. A.; Muller, E. A.; Olmon, R. L.; Martin, M. C.; Raschke, M. B. Ultrabroadband infrared nanospectroscopic imaging. *Proc. Natl. Acad. Sci. U.S.A.* **2014**, *111*, 7191−7196.

(26) Gerber, J. A.; Berweger, S.; O'Callahan, B. T.; Raschke, M. B. Phase-resolved surface plasmon interferometry of graphene. *Phys. Rev. Lett.* **2014**, *113*, 055502.

(27) Fei, Z.; Rodin, A. S.; Andreev, G. O.; Bao, W.; McLeod, A. S.; Wagner, M.; Zhang, L. M.; Zhao, Z.; Thiemens, M.; Dominguez, G.; Fogler, M. M.; Neto, A. H. C.; Lau, C. N.; Keilmann, F.; Basov, D. N. Gate-tuning of graphene plasmons revealed by infrared nano-imaging. *Nature* **2012**, *487* (7405), 82−85.

(28) Chen, J.; Badioli, M.; Alonso-Gonzalez, P.; Thongrattanasiri, S.; Huth, F.; Osmond, J.; Spasenovic, M.; Centeno, A.; Pesquera, A.; Godignon, P.; Zurutuza Elorza, A.; Camara, N.; Javier Garcia de Abajo, F.; Hillenbrand, R.; Koppens, F. H. L. Optical nano-imaging of gate-tunable graphene plasmons. *Nature* **2012**, *487* (7405), 77−81.

(29) Taniguchi, T.; Watanabe, K. Synthesis of high-purity boron nitride single crystals under high pressure by using Ba-BN solvent. *J. Cryst. Growth* **2007**, *303*, 525−529.

(30) Poddubny, A.; Iorsh, I.; Belov, P.; Kivshar, Y. Hyperbolic metamaterials. *Nat. Photonics* **2013**, *7*, 958−967.

(31) Mahan, G. D. *Many-Particle Physics*; Springer: 2000; pp 323−346.

(32) Hillenbrand, R.; Knoll, B.; Keilmann, F. Pure optical contrast in scattering-type scanning near-field microscopy. *J. Microsc. (Oxford, U.K.)* **2001**, *202*, 77−83.

(33) Atkin, J. M.; Berweger, S.; Jones, A. C.; Raschke, M. B. Nano-optical imaging and spectroscopy of order, phases, and domains in complex solids. *Adv. Phys.* **2012**, *61*, 745−842.

(34) Govyadinov, A. A.; Amenabar, I.; Huth, F.; Carney, P. S.; Hillenbrand, R. Quantitative measurement of local infrared absorption and dielectric function with tip-enhanced near-field microscopy. *J. Phys. Chem. Lett.* **2013**, *4*, 1526−1531.